

Review

Recent Advances in $\text{MnO}_x/\text{CeO}_2$ -Based Ternary Composites for Selective Catalytic Reduction of NO_x by NH_3 : A Review

Hao Sun and Soo-Jin Park *

Department of Chemistry, Inha University, 100 Inharo, Incheon 22212, Korea; sunhao92@naver.com

* Correspondence: sjpark@inha.ac.kr; Tel.: +82-32-876-7234; Fax: +82-32-867-5604

Abstract: Recently, manganese oxides (MnO_x)/cerium(IV) oxide (CeO_2) composites have attracted widespread attention for the selective catalytic reduction (SCR) of nitrogen oxides (NO_x) with ammonia (NH_3), which exhibit outstanding catalytic performance owing to unique features, such as a large oxygen storage capacity, excellent low-temperature activity, and strong mechanical strength. The intimate contact between the components can effectively accelerate the charge transfer to enhance the electron–hole separation efficiency. Nevertheless, $\text{MnO}_x/\text{CeO}_2$ still reveals some deficiencies in the practical application process because of poor thermal stability, and a low reduction efficiency. Constructing $\text{MnO}_x/\text{CeO}_2$ with other semiconductors is the most effective strategy to further improve catalytic performance. In this article, we discuss progress in the field of $\text{MnO}_x/\text{CeO}_2$ -based ternary composites with an emphasis on the SCR of NO_x by NH_3 . Recent progress in their fabrication and application, including suitable examples from the relevant literature, are analyzed and summarized. In addition, the interaction mechanisms between $\text{MnO}_x/\text{CeO}_2$ catalysts and NO_x pollutants are comprehensively dissected. Finally, the review provides basic insights into prospects and challenges for the advancement of $\text{MnO}_x/\text{CeO}_2$ -based ternary catalysts.

Keywords: $\text{MnO}_x/\text{CeO}_2$ composite; catalysis; NO_x reduction



Citation: Sun, H.; Park, S.-J. Recent Advances in $\text{MnO}_x/\text{CeO}_2$ -Based Ternary Composites for Selective Catalytic Reduction of NO_x by NH_3 : A Review. *Catalysts* **2021**, *11*, 1519. <https://doi.org/10.3390/catal11121519>

Academic Editors:
Bogdan Samojeden and
Teresa Grzybek

Received: 28 October 2021
Accepted: 13 December 2021
Published: 14 December 2021

Publisher's Note: MDPI stays neutral with regard to jurisdictional claims in published maps and institutional affiliations.



Copyright: © 2021 by the authors. Licensee MDPI, Basel, Switzerland. This article is an open access article distributed under the terms and conditions of the Creative Commons Attribution (CC BY) license (<https://creativecommons.org/licenses/by/4.0/>).

1. Introduction

Nitrogen oxides (NO_x) are mainly generated by human activities, such as automobile exhaust, fossil fuels combustion, and chemical industry emissions, which may induce multiple environmental problems, including acid rain, ozone depletion, and greenhouse effects [1–7]. With the gradual progression of modern industrialization and urbanization, NO_x emission has become a major environmental issue [8–10]. Therefore, NO_x removal by applying an eco-friendly and sustainable technology is urgently required [11,12]. The specific catalytic reduction (SCR) of NO_x with NH_3 is a widely used approach for the degradation of pollutants, and plays an important role in energy conservation and emission reduction [13–25].

Thus far, various catalytic materials has been explored for the degradation of pollutants. Among them, $\text{MnO}_x/\text{CeO}_2$ composites have been extensively employed as highly efficient catalysts for the reduction of NO_x with NH_3 because of their unique characteristics, such as their simple synthesis, stable chemical structure, and excellent low temperature efficiency [25–31]. The introduction of manganese cations into a ceria lattice immensely enhances oxygen mobility in mixed oxides. In addition, $\text{MnO}_x/\text{CeO}_2$ composites with hollow structures possess high NO_x storage capacity at low temperatures and excellent catalytic performance for the reduction of NO_x owing to the large specific surface area, sufficient active sites, and their characteristic confined microenvironment [32–44]. However, the catalytic activity of $\text{MnO}_x/\text{CeO}_2$ composites is still deficient due to their low sulfur resistance and poor thermal stability [25,45,46]. As a result, the hybridization of $\text{MnO}_x/\text{CeO}_2$ with other semiconductors has been widely applied to improve performance. Various efforts to enhance the catalytic activity of these materials, such as the loading of noble metals, doping with extraneous elements, modifying the surface morphology,

and fabricating heterojunction composites with other semiconductor materials, have been explored [47–54]. Among these, the fabrication of heterojunction composite systems can create more redox reaction sites and provides higher tenability and controllability, which is an effective strategy for improving the catalytic activity applied in environmental remediation [55–58]. Thus, combining $\text{MnO}_x/\text{CeO}_2$ with other semiconductors has been extensively studied. For instance, Zhang et al. [59] prepared $\text{MnO}_x\text{-CeO}_2/\text{TiO}_2$ ternary catalysts that showed greatly enhanced catalytic activity for removing NO_x with NH_3 at low temperature compared to single semiconductor materials. In addition, Wang et al. [60] developed $\text{MnO}_x/\text{CeO}_2/\text{Al}_2\text{O}_3$ hybrid composite catalysts that achieved a NO_x conversion greater than 90% due to their enhanced pore structure and a large specific surface area.

Presently, reviews of the preparation and application of $\text{MnO}_x/\text{CeO}_2$ -based ternary catalysts are still rare. In this review, the research progress of $\text{MnO}_x/\text{CeO}_2$ -based ternary composites and their use in the catalytic reduction of NO_x with NH_3 are summarized and proposed. Finally, we present some perspectives of the present circumstances and further prospects to further improve the understanding and extensive application of $\text{MnO}_x/\text{CeO}_2$ -based ternary nanocomposites.

2. The Preparation and Catalytic Mechanism of $\text{MnO}_x/\text{CeO}_2$

2.1. The Preparation of $\text{MnO}_x/\text{CeO}_2$

$\text{MnO}_x/\text{CeO}_2$ can possess different structures and chemical performances incurred by various synthetic approaches and designs. Among them, the co-precipitation method is an important way to construct composites owing to the simple operation, manageable reaction conditions, and good products with uniform composition. In addition, the morphology and structure of the sample can be controlled by adjusting the reaction conditions, such as the solution pH value, temperature, etc. For instance, Ye et al. [61] successfully synthesized $\text{MnO}_x/\text{CeO}_2$ catalyst via a conventional co-precipitation method by blending manganese nitrate ($\text{Mn}(\text{NO}_3)_2$) with cerium nitrate ($\text{Ce}(\text{NO}_3)_3 \cdot 6\text{H}_2\text{O}$) at room temperature. In detail, a 12.5 wt.% ammonia solution was added dropwise to a solution containing 50 wt.% $\text{Mn}(\text{NO}_3)_2$ and $\text{Ce}(\text{NO}_3)_3 \cdot 6\text{H}_2\text{O}$ at various molar ratios. The pH of the resulting solution was kept at 10.5 and stirred for 2 h. Finally, the as-obtained samples were collected by filtered washing several times with deionized water and ethyl alcohol, drying for 12 h at 105 °C, and the calcined for 6 h at 650 °C under an air atmosphere Qi et al. [27] developed a novel $\text{MnO}_x/\text{CeO}_2$ catalyst that achieved 95% NO conversion at 150 °C. Li et al. [62] reported $\text{MnO}_x/\text{CeO}_2$ prepared via a similar procedure, reaching 99% NO_x conversion at 170 °C and 80% NO conversion rate in the temperature range of 120–275 °C; compared to the above-mentioned catalysts, it possess highest NO_x conversion efficiency. Moreover, the main advantage of the hydrothermal method is that well-crystallized products can be easily obtained. Liu et al. [26] developed a novel $\text{MnO}_x/\text{CeO}_2$ catalyst with a shell-in-shell microspherical structure through a one-step hydrothermal method. In this process, 3.0 g of urea was completely dissolved in 100 mL deionized water. Subsequently, a certain amount of $\text{CeCl}_3 \cdot 7\text{H}_2\text{O}$ and $\text{Mn}(\text{NO}_3)_2$ were added under continuous stirring to form a clear solution. Afterward, the obtained mixture was transferred to a Teflon-sealed stainless-steel autoclave and heated for 180 °C for 20 h. The final product was filtered, washed with deionized water several times, and then dried at 80 °C for 12 h. Li et al. [63] evaluated a novel $\text{MnO}_x\text{-CeO}_2$ nanosphere catalyst with an assembled structure. It showed that the catalyst achieved a NO conversion about 100% in the entire 125–250 °C range. Moreover, other approaches, such as chemical deposition and oxidation-reduction reaction, have also been frequently applied to synthesize $\text{MnO}_x/\text{CeO}_2$ -based nanocomposites [35,64].

As a result, it can be found that the preparation means and morphology of $\text{MnO}_x/\text{CeO}_2$ can affect the performance of catalysts. The morphology and structure of a sample can be controlled by adjusting the reaction conditions, such as solution pH value, temperature, etc. The $\text{MnO}_x/\text{CeO}_2$ catalyst prepared using the co-precipitation method exhibited a higher catalytic activity. Relatively, the main advantage of the hydrothermal method is that

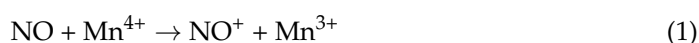
well-crystallized product can be easily obtained. The preparation of MnO_x/CeO₂ binary nanocomposites using different methods is summarized in Table 1.

Table 1. The preparation of MnO_x/CeO₂ binary catalysts.

Catalyst	Constructing Strategy	Precursors	Catalytic Activity	Reference
MnO _x /CeO ₂	co-precipitation method	Mn(NO ₃) ₂ Ce(NO ₃) ₃ ·6H ₂ O	NO and toluene conversion > 60% temperature < 300 °C	[61]
	oxidation-reduction reaction	Ce(NO ₃) ₃ ·6H ₂ O KMnO ₄	MnO _x -CeO ₂ -B achieve 96% NO _x conversion at 100 °C at a space velocity of 30000 h ⁻¹	[35]
	co-precipitation method	Mn(NO ₃) ₂ Ce(NO ₃) ₃	MnO _x (0.4)-CeO ₂ (500) achieve 95% NO _x conversion at 150 °C MnO _x -CeO ₂ microsphere catalyst presented	[27]
	hydrothermal method	CeCl ₃ ·7H ₂ O Mn(NO ₃) ₂	higher catalytic activity at low temperatures than catalyst without shell-in-shell microsphere structure	[26]
	chemical deposition method	Mn(CH ₃ COO) ₂ Ce(NO ₃) ₃	CeO ₂ /MnO _x = 0.6 exhibited a relatively high conversion of NO	[64]
	hydrothermal method	Ce(NO ₃) ₃ ·6H ₂ O Mn(CH ₃ COO) ₂ ·4H ₂ O	The NO conversion of MCN achieves a conversion of about almost 100% in the whole 125–250 °C range The NO _x conversion of 6Mn4Ce-C reached its maximum of 99% at 170 °C; and it's NO conversion rate remained >80% at the temperature range of 120–275 °C.	[63]

2.2. The Catalytic Mechanism of MnO_x/CeO₂ for SCR with NH₃

A catalyst is a material that can potentially be used for environment purification. Electrons and holes are shifted to the surface of the catalyst and produce active species for redox reactions to remove pollutants. Figure 1 describes the mechanism for the SCR process of MnO_x-CeO₂ catalyst. There are two reaction mechanisms for the NH₃-SCR process over the MnO_x-CeO₂ catalyst, the Eley–Rideal (E–R) mechanism and Langmuir–Hinshelwood (L–H) mechanism [65,66]. These depend mainly on the adsorption state of the NH₃ species react with the adsorbed or gaseous NO_x. The NH₃-SCR over the MnO_x-CeO₂ catalyst mainly followed the L–H mechanism rather than the E–R mechanism [67,68]. The Ce³⁺ and Mn³⁺ sites in the MnO_x/CeO₂ can improve the transfer efficiency of the activated oxygen molecules to generate surface-adsorbed oxygen species. Firstly, the NO molecules react with the Mn⁴⁺ to generate NO⁺. The obtained NO⁺ can further transformed into NO₂ through a combination of surface-adsorbed oxygen species. In the next moment, the adsorbed NH₃ species combine with surface activated oxygen to form NH₂⁻. Finally, N₂ and H₂O are obtained through the reaction of NO₂ and NH₂⁻ [45]. The SCR reaction followed the L–H mechanism, which exhibited excellent catalytic performance. The NH₃ species reacting with the adsorbed or gaseous NO depends mainly on the adsorption state, and their adsorption on the catalyst surface is the critical step in SCR with NH₃ [69–71]. The reaction pathways can be described using (1)–(4):



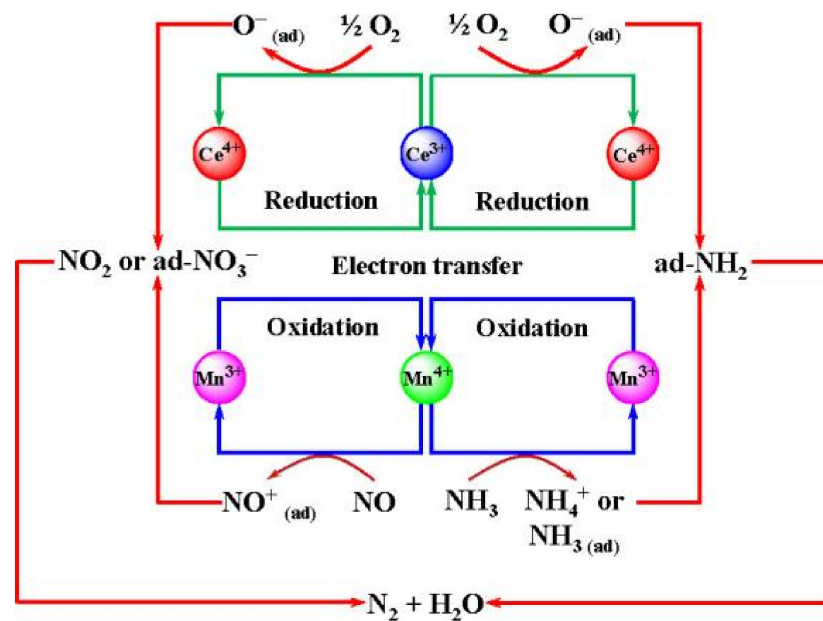


Figure 1. Mechanism for the SCR process of MnO_x/CeO₂. Reproduced with permission from Reference [45]; copyright (2017), Elsevier.

The catalytic activity of MnO_x/CeO₂ greatly hinges on its abundant active sites, specific surface area, and unique morphology [31,72–74]. In addition, MnO_x/CeO₂ with hollow structures improved catalytic activity, thereby making it effective at removing contaminants.

3. The Resistance Effect to H₂O and SO₂

Water vapor is able to destroy the acid sites of a catalyst to generate the poisoning effect on SCR, especially at low temperatures. When the temperature rises, the catalyst can be reactivated with a reduction in the inhibition effect. Even under dry conditions, the catalytic activity is still affected by the H₂O produced by SCR reactions. Water molecules in the catalytic process are regarded as an important factor. For the poisoning of SO₂, the effect of SO₂ in low-temperature can result from the formation of ammonium sulfate species on catalyst surface, causing deactivation of the SCR. In flue gas containing both H₂O and SO₂, the resistance effects is more significant. Qi et al. [27] found that the conversion of NO changed from 98 to 95% in the presence of SO₂ and H₂O at low temperatures. Li et al. [35] proposed that the NO_x conversion decreases from 100% to about 84% in 8 h and the catalytic activity restores up to 90% after adding SO₂. Therefore, introducing water-resistant and sulfur-resistant materials may be an effective approach to solve the poisoning of H₂O and SO₂.

4. The Construction of MnO_x/CeO₂-Based Ternary Catalysts

The synthetic approaches for catalysts are closely related to catalytic performance. Different preparation methods can strongly impact on the structure, specific surface area, absorption, and porosity of catalysts. These synthesis methods mainly include hydrothermal, precipitation, sol–gel, and impregnation. For MnO_x/CeO₂-based ternary catalysts, Table 2 summarized the type of catalysts, preparation method, reaction conditions, and catalytic performance.

Table 2. Summary of MnO_x/CeO₂-based ternary catalysts for NO_x removal.

Catalyst	Preparation Method	Testing Condition	Catalytic Performance	Reference
MnO _x /CeO ₂ /graphene	Hydrothermal method	A fixed bed continuous flow reactor at 40–160 °C, the GHSV of 24,000 h ⁻¹ .	NO _x conversion on MnO _x -CeO ₂ (8:1)/GR catalyst achieve 99.3% at 80 °C N ₂ selectivity nearly 95% at 80 °C	[25]
VO _x /MnO _x /CeO ₂	Impregnation methods	Catalysts (200 mg, 40–60 mesh), a GHSV of 160,000 h ⁻¹ , a flow rate of 600 mL/min	NH ₃ -SCR activity (NO conversion > 95%)	[30]
MnO _x /CeO ₂ /MOF	Hydrothermal method	50 mg catalyst, the flow rate of 50 mL/min, GHSV of 60,000 mL/g _{cat} h.	Toluene conversion was 86%	[34]
MnO _x /CeO ₂ /ZrO ₂	Precipitation method	The flow rate of 420 mL/min, the GHSV by volume was 10,000 h ⁻¹ .	NO _x conversion is over 80%	[46]
MnO _x /CeO ₂ /reduced graphene oxide	Hydrothermal method	The flow rate was 500 mL·min ⁻¹ , a GHSV of 30,000 h ⁻¹ .	NO _x conversion (~99%) could be attained at 220 °C	[75]
SnO ₂ /MnO _x /CeO ₂	Precipitation method	0.20g catalyst, a gas flow rate of 100 mL min ⁻¹ , GHSV of 3.5 × 10 ⁴ h ⁻¹	More than 98% NO conversion was obtained at 80 °C and nearly 100% NO conversion at the temperature range of 110–230 °C	[76]
MnO _x /CeO ₂ /Al ₂ O ₃	Sol-gel method	100 mg of catalyst, the reactor temperature was ramped to 650 °C.	The NO oxidation activities achieves 99%	[77]
MnO _x /CeO ₂ /SBA-15	Sol-gel method	Catalyst (200 mg, 10–20 mesh), reaction was run from 100 to 650 °C	soot oxidation with 100% selectivity to CO ₂	[78]
Ba/MnO _x /CeO ₂	Impregnation method	10 mg of catalysts, test was at 600 °C (heating rate 15 °C/min)	The amount of NO _x desorbed from BaMnCe within the temperature interval of 350–450 °C is 2.8 times of that MnCe	[79]
MnO _x /CeO ₂ /TiO ₂	Impregnation method	0.20 g catalyst (20–40 mesh), a GHSV of 30,000 h ⁻¹	the NO _x removal efficiency achieves up to 77.1%	[79]
MnO _x /CeO ₂ /Cu-SSZ-13	impregnation method	N ₂ was the balanced gas, and total flow rate = 300 mL min ⁻¹	The NO _x conversions were above 90% from 125 °C to 450 °C	[80]
MnO _x /CeO ₂ @TiO ₂	hydrothermal method	The air flow rate was 1600 mL/min and the airspeed was 24,000 h ⁻¹	The NO _x conversion of MnO _x /CeO ₂ @TiO ₂ reaches around 100% at 140 °C. The N ₂ selectivity of MnO _x /CeO ₂ @TiO ₂ remains above 95% from 40 to 200 °C.	[81]
MnO _x /CeO ₂ /TiO ₂	Co-precipitation method	The GHSV was 27 000 h ⁻¹ , and the catalytic temperature was at the range of 80–300°C.	The NO _x conversions reaches 87% at 150 °C and the NO conversion is 85% at the temperature of 300 °C	[82]
MnO _x /CeO ₂ /VO _x	impregnation method	The catalyst (200 mg, 40–60 mesh), the GHSV was 160,000 h ⁻¹	VO _x -MnO _x /CeO ₂ -R achieve > 95 % NO conversion at ~220 °C.	[83]
MnO _x /CeO ₂ /TiO ₂	impregnation method	The total flow was 500 cc/min, and GHSV of 60,000 h ⁻¹	Mn(20)/Ce(4)-TiO ₂ catalyst obtained 90% NO _x conversion at 180 °C and >94% N ₂ selectivity	[84]

4.1. Hydrothermal Methods

Hydrothermal methods are the most simple and economical for large-scale synthesis and make it easy to obtain well-crystallized products by adjusting reaction conditions [85–88]. $\text{MnO}_x/\text{CeO}_2$ -based catalysts obtain a good morphology and structure due to the high temperature and pressure in the hydrothermal system.

For instance, novel $\text{MnO}_x/\text{CeO}_2$ /graphene ternary catalysts was prepared as follows [25]: 0.01 g graphene was first dispersed in 100 mL deionized water, and then certain amounts of $\text{Mn}(\text{NO}_3)_2 \cdot 3\text{H}_2\text{O}$ and $\text{Ce}(\text{NO}_3)_3 \cdot 6\text{H}_2\text{O}$ were added to the suspension. After that, ammonia at 20 wt.% was added to the solution under constant ultrasonic agitation. The mixture was then transferred into a Teflon-sealed autoclave and heated at 130 °C for 12 h. The obtained product was centrifugated and washed with deionized water several times, and then dried at 100 °C for 12 h. For comparison, other samples (different Mn/Ce molar ratios) were prepared under the same conditions. Sun et al. [34] fabricated $\text{MnO}_x/\text{CeO}_2/\text{MOF}$ catalysts for catalytic reaction. Briefly, a certain amount of $\text{MnCl}_2 \cdot 4\text{H}_2\text{O}$, $\text{Ce}(\text{NO}_3)_3 \cdot 6\text{H}_2\text{O}$, and 2,5-dihydroxyterephthalic acid were added to dimethyl furan-ethanol-water. Subsequently, the suspension was transferred into a Teflon-lined stainless-steel autoclave, and heated in an oven at 135 °C for 24 h. The product was washed with methanol, and dried in a 80 °C vacuum oven. Finally, samples was obtained through calcination at 550 °C in air. Zhu et al. [75] produced $\text{MnO}_x/\text{CeO}_2$ /reduced graphene oxide that exhibited a high SCR efficiency via a one-step hydrothermal method. In the synthesis process, aqueous graphene oxide was dissolved in deionized water and ammonia solution was added dropwise to the solution to keep the pH value at 11.5. An aqueous solution of $\text{Mn}(\text{NO}_3)_2$ and $\text{Ce}(\text{NO}_3)_3 \cdot 6\text{H}_2\text{O}$ was then added, followed by stirring at room temperature. After that, the mixture was transferred to a Teflon-lined autoclave and heated in an oven at 180 °C for 12 h. The final product was obtained and washed several times with deionized water. However, the hydrothermal method cannot control the number of nanocomposites exactly, making it prone to agglomeration

4.2. Precipitation Method

Precipitation is the formation of a solid from a homogeneous solution caused by a precipitating agent. This method is widely applied to prepare catalysts because of the controllable reaction conditions, effortless operation, and well-proportioned products [89,90], and is the most common approach for constructing $\text{MnO}_x/\text{CeO}_2$ -based ternary composites.

For instance, a mixed solution containing carbamide solution, NH_3 (25 wt.%), and hydrogen peroxide was continuously added into aqueous solutions of titanium(IV) sulfate ($\text{Ti}(\text{SO}_4)_2$), manganese acetate ($\text{C}_4\text{H}_6\text{MnO}_4 \cdot 4\text{H}_2\text{O}$), and Ce, Fe, and Ni nitrates. Subsequently, the resulting precipitant was collected by centrifugation, followed by washing with ethyl alcohol and deionized water. Finally, the mixture was dried at 105 °C for 12 h, and then calcined at 450 °C in a muffle furnace. Furthermore, Chang et al. [76] reported $\text{SnO}_2/\text{MnO}_x/\text{CeO}_2$ catalysts for SCR of NO_x with ammonia. In their technique, $(\text{NH}_4)_2\text{CO}_3$ was dispersed as a precipitator into a mixed solution of SnCl_4 , $\text{Mn}(\text{NO}_3)_2$, and $\text{Ce}(\text{NO}_3)_3$. The obtained paste was collected by ultrasound for 2 h, followed by subsequent filtration, washing with DI water, and calcination at 500 °C for 6 h. A catalytic material, $\text{WO}_3\text{-ZrO}_2$, was synthesized using the precursors ammonium metatungstate and zirconyl nitrate hydrate at the appropriate ratios [46], and the preparation procedure is shown in Figure 2.

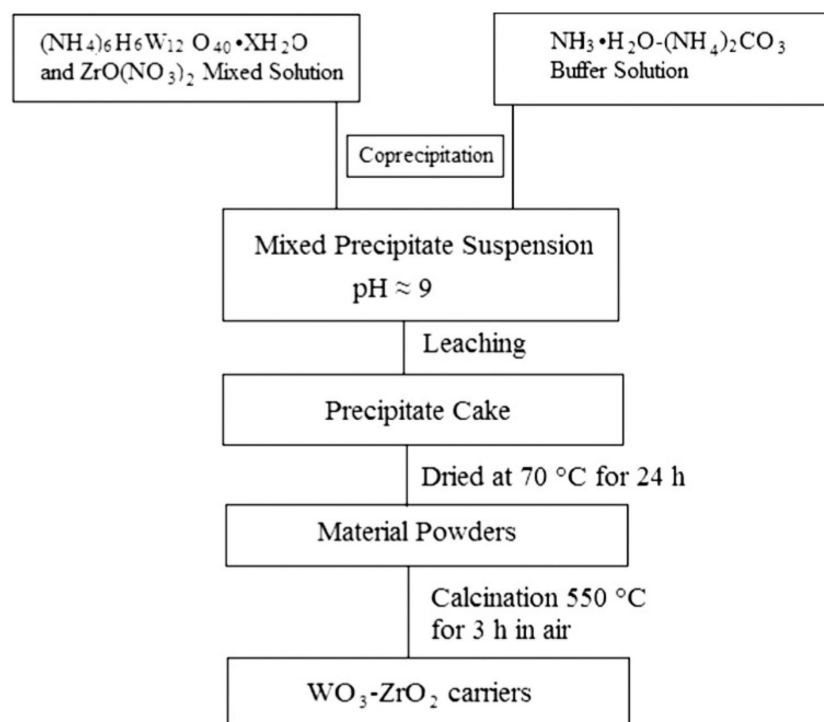


Figure 2. Preparation procedure of the carrier catalysts. Reproduced with permission from Reference [46]; copyright (2012), Elsevier.

4.3. Sol–Gel Methods

The sol–gel technique can be used to obtain highly pure materials and tune their composition due to its low cost, energy, and time consumption [91–93]. This approach is well-established for the preparation of novel metal oxide nanoparticles and mixed-oxide materials, and is beneficial for the stability of the products. Therefore, sol–gel methods have been widely applied for constructing $\text{MnO}_x/\text{CeO}_2$ -based ternary nanocomposites.

A novel $\text{MnO}_x/\text{CeO}_2/\text{Al}_2\text{O}_3$ composite has been synthesized for soot oxidation in the presence of NO_x through a facile sol–gel process involving $\text{Ce}(\text{NO}_3)_3 \cdot 6\text{H}_2\text{O}$ and manganese acetate as precursors [77]. In brief, these were dissolved, and the suspension was then stirred sufficiently to form a porous gel that was dried at 110 °C overnight followed by calcination at 500 °C under static air in a muffle furnace. Zhang et al. [78] prepared $\text{MnO}_x/\text{CeO}_2/\text{SBA-15}$ (Santa Barbara Amorphous-15) catalysts with a 3D network structure using a sol–gel method for NO_x -assisted soot combustion. Typically, certain amounts of $\text{Ce}(\text{NO}_3)_3 \cdot 6\text{H}_2\text{O}$ and $\text{Mn}(\text{NO}_3)_2$ in aqueous solution were first added to anhydrous ethanol. After that, 1.00 g of SBA-15 was added dropwise to the mixed suspension, which was then dried at room temperature followed by calcination at 500 °C for 5 h in air.

4.4. Impregnation Methods

Impregnation methods are fast, low cost, and allow controllable configuration in advance by tweaking some parameters, such as concentration and the temperature of the precursor [94–96]. For instance, Wu et al. [97] prepared $\text{Ba}/\text{MnO}_x/\text{CeO}_2$ catalysts via impregnation to be employed for soot oxidation with heat transfer limitations. The composites were impregnated with an aqueous solution of barium acetate ($\text{Ba}(\text{Ac})_2$). The final products were obtained by heating at 110 °C for 12 h, followed by calcination at 550 °C in air. In addition, $\text{MnO}_x/\text{CeO}_2/\text{TiO}_2$ mixed-oxide catalysts have been synthesized with differing $\text{CeO}_2/\text{TiO}_2$ ratios via impregnation for application in low-temperature catalytic ozonation of NO_x into HNO_3 [79]. A conventional $\text{MnO}_x/\text{CeO}_2$ supported with VO_x (vanadium oxides) catalyst (denoted as $\text{VO}_x/\text{MnO}_x/\text{CeO}_2$) was synthesized via a wet-impregnation method (Figure 3) [30]. In this typical synthesis, the mixture

of $\text{Ce}(\text{NO}_3)_3 \cdot 6\text{H}_2\text{O}$ and KIT-6 were calcinated at $500\text{ }^\circ\text{C}$ for 4 h in air. After cooling to ambient temperature, the samples were centrifuged twice with NaOH to remove the KIT-6 template. Finally, 3-D mesoporous CeO_2 supported with VO_x and MnO_x binary metal oxides was prepared.

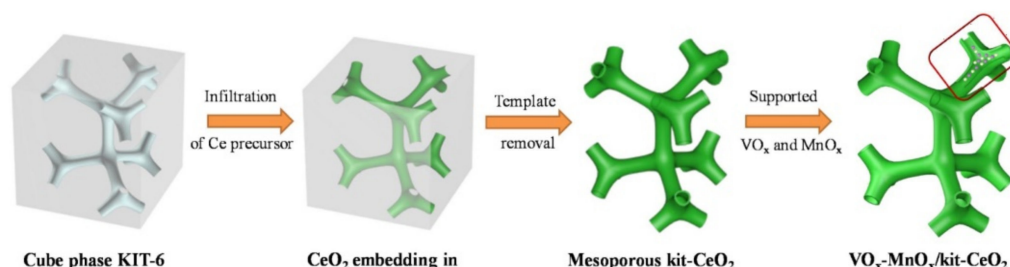


Figure 3. Schematic representation of the synthesis processes of mesoporous $\text{VO}_x\text{-MnO}_x/\text{CeO}_2$. Reproduced with permission from Reference [30]; copyright (2020), Elsevier.

5. The Application for SCR of NO_x by NH_3

In recent years, NO_x , as an atmospheric pollutants from industrial discharge, has widely aroused public concern and resulted in a serious threat to human health and life [98–104]. Therefore, removing NO_x from air is imperative. Considerable attention has been paid to catalytic technologies owing to their excellent properties, such as high efficiency and low cost. Therefore, some articles about producing $\text{MnO}_x/\text{CeO}_2$ composites for the SCR of NO_x with NH_3 are summarized here.

5.1. $\text{MnO}_x/\text{CeO}_2$ Binary Catalyst for SCR of NO_x by NH_3

Ye et al. [61] developed $\text{MnO}_x/\text{CeO}_2$ using a conventional co-precipitation method to remove NO_x by SCR with NH_3 to leave N_2 . The catalytic performance of $\text{MnO}_x/\text{CeO}_2$ composites decrease significantly in the presence of toluene, which is attributed to the competitive adsorption of toluene and the deposition of by-products on the catalyst surface. Meanwhile, toluene adsorption enhanced the formation of oxygen vacancies and increased the unfavored oxidation reactions of NH_3 , leading to a decrease in N_2 selectivity. Novel $\text{MnO}_x/\text{CeO}_2$ hollow nanotubes were applied to the low-temperature SCR of NO_x with NH_3 [35]. It was demonstrated that $\text{MnO}_x/\text{CeO}_2$ nanocomposites exhibited best conversion efficiency of NO_x at $100\text{ }^\circ\text{C}$, and had superior resistance to H_2O and SO_2 . According to the analysis results, the excellent NO_x catalytic property of the $\text{MnO}_x/\text{CeO}_2$ catalyst could be ascribed to the uniform distribution and abundant content of active species, especially the hollow porous architectures that provided higher specific surface area.

Qi et al. [27] employed a co-precipitation method for the preparation of $\text{MnO}_x/\text{CeO}_2$ mixed oxides. X-ray diffraction (XRD), surface area measurements, and Fourier-transform infrared (FTIR) spectroscopy were employed to characterize $\text{MnO}_x/\text{CeO}_2$ catalyst. It was found that Mn-Ce mixed-oxide catalyst yielded 95% NO removal efficiency at $150\text{ }^\circ\text{C}$ at a space velocity of $42,000\text{ h}^{-1}$. With increasing manganese weight ratios, NO conversion efficiency gradually increased, but decreased at higher manganese contents. The $\text{MnO}_x/\text{CeO}_2$ heterojunction represented an improved catalytic activity on account of the adsorption of NH_3 on the Lewis acid sites of the catalyst, followed by reaction with nitrite species to produce N_2 .

More recently, Liu et al. [26] prepared novel $\text{MnO}_x/\text{CeO}_2$ shell-in-shell microspheres that showed better catalytic activity for SCR of NO compared with the CeMnO_x catalyst without the core-shell structure. $\text{MnO}_x/\text{CeO}_2$ catalysts present great potential in terms of catalytic reduction of NO_x due to the oxygen storage and redox property. The TEM and HRTEM images showed that a small hollow sphere was located in the inside of a big hollow sphere to construct a double-shelled hollow sphere (Figure 4). On the basis of the data from XPS measurements, it was observed that $\text{MnO}_x/\text{CeO}_2$ is composed of MnO_x and CeO_2 .

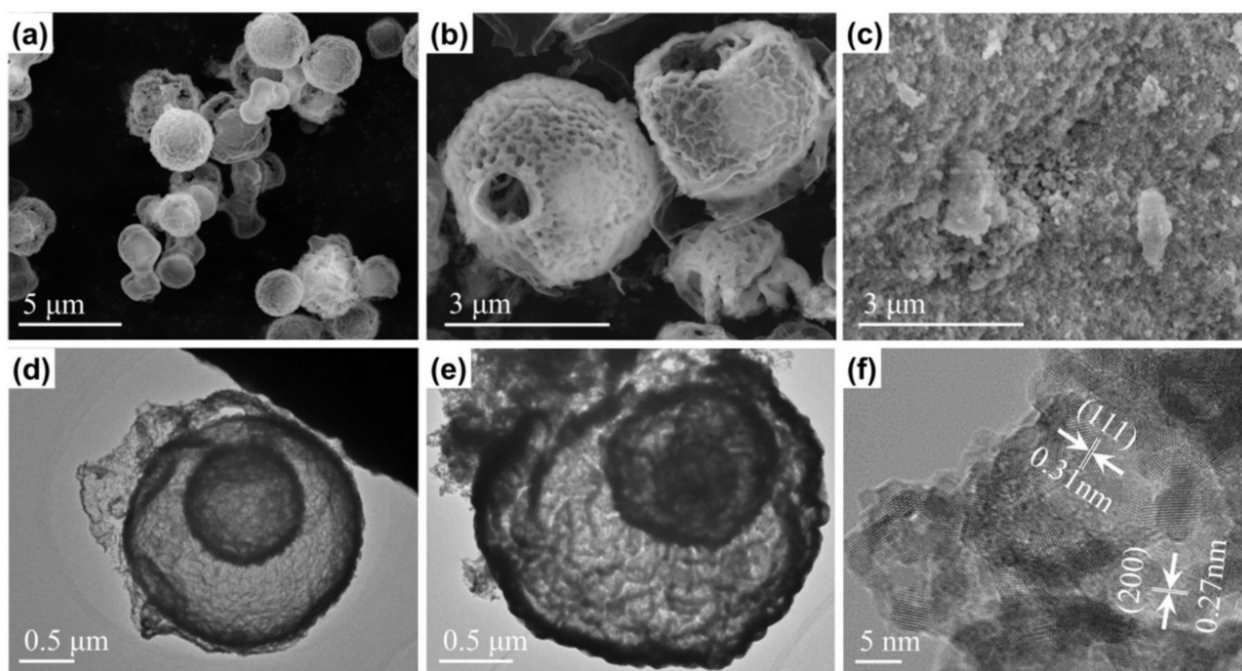


Figure 4. SEM images of Mn-CeO₂ (HT) (a,b) and Mn-CeO₂ (CP) (c), and TEM image (d,e) and high resolution TEM image (f) of Mn-CeO₂ (HT). Reproduced with permission from Reference [26]; copyright (2016), Elsevier.

Li et al. [63] reported that a novel MnO_x/CeO₂ nanosphere catalyst with assembled structure from tiny particle exhibited excellent catalytic performance for the reduction of NO_x. Compared to pure MnO_x and CeO₂, MnO_x/CeO₂ nanosphere catalyst show a superior DeNO_x performance because of the higher specific surface area, better redox behavior, and larger concentration of surface active oxygen species. The stability of MnO_x/CeO₂ nanosphere NH₃-SCR catalyst achieved the best effect at 150 °C for long time. In addition, the pore diameter and BET surface area of the composite were higher than those of the single MnO_x and CeO₂ samples. The results of the study suggested that control of defined structural morphology can improve NH₃-SCR performance.

Li et al. [62] successfully synthesized a mesoporous MnO_x/CeO₂ composites through a traditional co-precipitation route. The prepared catalyst exhibited enhanced performance for NO_x conversion, which can be attributed to its smaller pores, amorphous structure, and moderate amount of surface Mn³⁺/oxygen species. Moreover, the porous structure of composites provided a larger surface area and made the adsorption and diffusion of reactant molecules easy to conduct on the surface of catalysts. The MnO_x/CeO₂ nanocomposite exhibited higher catalytic activity than pure MnO_x and CeO₂ for the SCR of NO with NH₃.

Huang et al. [64] reported a CeO₂/MnO_x catalyst with a core-shell structure was prepared via a facile a chemical deposition method. The TEM images of the CeO₂/MnO_x heterostructure identified a distinct core-shell structure and a uniform size of the CeO₂/MnO_x and MnO_x nanoparticles. The improvement in SCR performance is attributed to the uniform core-shell structure, the high crystalline α-MnO₂, as well as the high concentration of Mn⁴⁺ and Ce³⁺ in the CeO₂/MnO_x solid structure.

5.2. MnO_x/CeO₂ Based Ternary Catalysts for SCR of NO_x

The catalytic technique has attracted a great deal of attention and is widely investigated to apply SCR of NO using NH₃. Especially, MnO_x/CeO₂-based ternary catalyst can significantly promote catalytic activity for environmental pollution, including the reduction of NO_x [20,105]. Therefore, the application and properties of MnO_x/CeO₂-based ternary composites are summarized and discussed.

Sheng et al. [25] developed $\text{MnO}_x/\text{CeO}_2/\text{graphene}$ catalysts prepared via a hydrothermal method using different molar ratios of Mn/Ce active components. The results in the morphology and microstructure indicated that manganese and cerium oxides were uniformly dispersed on the surface of graphene. The $\text{MnO}_x/\text{CeO}_2$ (8:1)/GR displayed the best catalytic activity, and a high N_2 selectivity, which are attributed to the high content of chemisorbed oxygen on the surface, abundant active sites, and the synergistic effect between $\text{MnO}_x/\text{CeO}_2$ and the graphene support. Hence, the excellent catalytic performance of $\text{MnO}_x/\text{CeO}_2/\text{GR}$ composites at low temperature were widely applied in controlling NO_x emissions from flue gas.

Liu et al. [80] successfully developed a novel $\text{MnO}_x/\text{CeO}_2$ supported on Cu-SSZ-13 catalyst through an impregnation method. The Mn-Ce/Cu-SSZ-13 possessed higher catalytic activities than Cu-SSZ-13 and Mn-Ce for NO_x conversions because the bridging nitrates were adsorbed onto the surface and then converted to monodentate nitrates. Therefore, ternary composites can obtain more active species for the SCR reaction at low temperatures.

Recently, Ma et al. [81] reported the synthesis of $\text{MnO}_x/\text{CeO}_2/\text{TiO}_2$ core-shell composites. TEM and high-resolution TEM images reveal that TiO_2 was distributed on the surface of $\text{MnO}_x/\text{CeO}_2$ nanorods to form the core-shell structure. $\text{MnO}_x/\text{CeO}_2/\text{TiO}_2$ showed excellent catalytic performance due to abundant active sites, strong redox capability, along with a large specific surface area and pore volume. Meanwhile, the TiO_2 shell of $\text{MnO}_x/\text{CeO}_2/\text{TiO}_2$ further promotes catalytic activity and physicochemical properties.

A synthesized $\text{MnO}_x/\text{CeO}_2/\text{Al}_2\text{O}_3$ (aluminum oxide) composite catalyst achieved 90% NO_x conversion from 150–300 °C [60]; its BET surface area and pore volume were approximately 207.5 m^2/g and 0.23 cm^3/g , respectively, while the $\text{MnO}_x/\text{CeO}_2/\text{Al}_2\text{O}_3$ ternary heterojunctions remarkably improved the catalytic performance and provided good stability through the large intimate interfacial contacts among the MnO_x , CeO_2 , and Al_2O_3 constituents.

Zhu et al. [75] reported the fabrication of 3D $\text{MnO}_x/\text{CeO}_2$ nanoparticles/reduced graphene aerogel (RGA) via a facile one-step hydrothermal method. The $\text{MnO}_x/\text{CeO}_2$ nanoparticles were uniformly distributed on graphene nanosheets to form self-assembling 3D interconnected networks. The composites showed significantly enhanced catalytic performance compared to $\text{MnO}_x/\text{CeO}_2$ nanoparticles (99% NO_x conversion at 220 °C). Therefore, $\text{MnO}_x/\text{CeO}_2$ -based ternary composite materials have great prospects for the SCR of NO_x at low temperatures. A schematic of the catalytic mechanism of $\text{MnO}_x/\text{CeO}_2/\text{RGA}$ is shown in Figure 5.

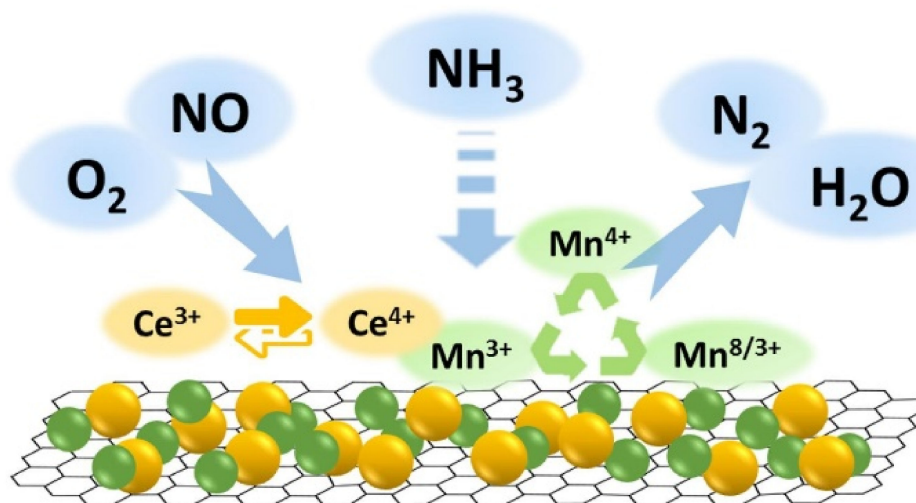


Figure 5. The schematic diagram of the catalytic mechanism of $\text{MnO}_x\text{-CeO}_2/\text{RGA}$ Reproduced with permission from Reference [75]; copyright (2019), Elsevier.

Zhang et al. [82] successfully developed a $\text{MnO}_x/\text{CeO}_2/\text{TiO}_2$ catalysts for SCR of NO with NH_3 at low temperatures. The results of BET show that the Mn-Ce/TiO₂ ternary catalyst has a large specific surface area and pore volume, which provided abundant active sites for improved catalytic activity. The XPS spectra of the prepared $\text{MnO}_x\text{-CeO}_2/\text{TiO}_2$ was used to analyze the surface chemical and valence states, which demonstrated the formation of heterojunction. In addition, it found that the low-temperature SCR performance was prominently enhanced. Meanwhile, NO conversion efficiency achieved the best effect in the temperature range of 150–300 °C. Figure 6 depicts the K^+ poisoning process of the catalyst.

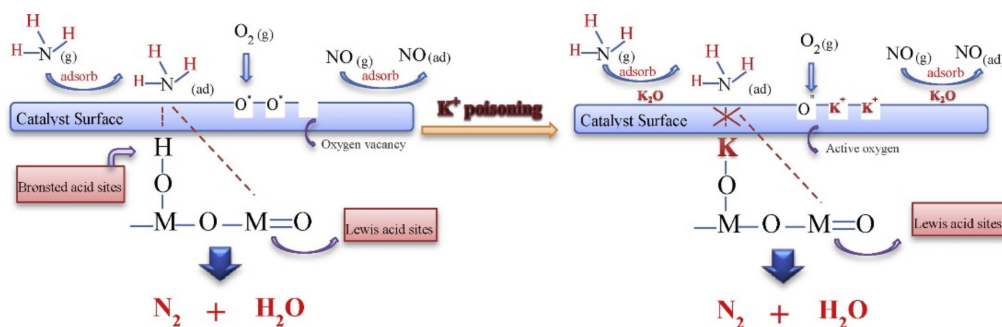


Figure 6. K^+ poisoning process of the catalyst. Reproduced with permission from Reference [82]; copyright (2014), Elsevier.

$\text{MnO}_x/\text{CeO}_2/\text{ZrO}_2$ monolith catalysts with a WO_3 content of 10 wt.% were fabricated using a co-precipitation method, which had the best catalytic activity and the widest reaction window [46]. In addition, it possessed a better thermal stability and SO_2 tolerance than pure $\text{MnO}_x/\text{CeO}_2$ materials. NO_x conversion was more than 80% in the low temperature range at the space velocity of 10,000 h^{-1} .

The construction of novel $\text{MnO}_x/\text{CeO}_2/\text{VO}_x$ catalysts was applied for selective catalytic reduction of NO_x by NH_3 [83]. The NH_3 -SCR performance of the catalytic experiment indicated that improved catalytic activity was achieved through the formation of $\text{MnO}_x/\text{CeO}_2/\text{VO}_x$ heterojunctions. The possible mechanisms of the $\text{VO}_x\text{-MnO}_x/\text{CeO}_2$ catalyst are shown in Figure 7.

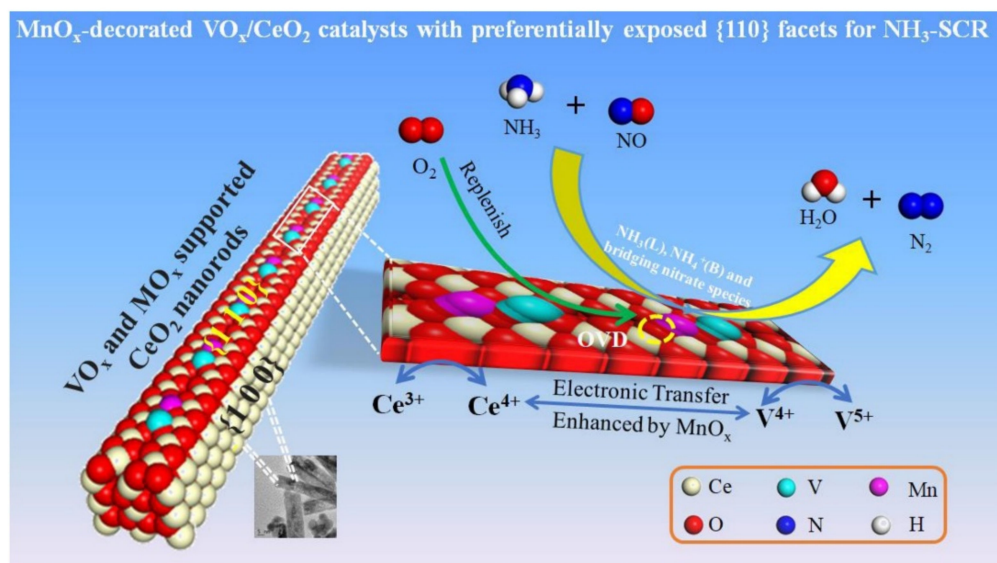


Figure 7. The possible mechanism of the $\text{VO}_x\text{-MnO}_x/\text{CeO}_2$ catalyst. Reproduced with permission from Reference [83]; copyright (2020), Elsevier.

In research conducted by Liu et al. [76], $\text{MnO}_x/\text{CeO}_2/\text{SnO}_2$ catalysts were prepared via a co-precipitation method for NH_3 -SCR reaction. The composite catalyst (10 wt.% of Sn

on $\text{MnO}_x/\text{CeO}_2$) displayed optimal catalytic activity in a temperature range of 80–230 °C. The remarkable catalytic activity was likely attributed to the enhanced Lewis acid sites created by surface sulfation during the SO_2 -containing SCR reaction.

Wu et al. [30] employed an efficient wet impregnation method for the fabrication of heterojunction $\text{VO}_x\text{-MnO}_x/\text{CeO}_2$ nanocomposites. TEM and HRTEM analyses were employed to investigate the microstructure and morphology of $\text{VO}_x\text{-MnO}_x/\text{CeO}_2$ (Figure 8). The ternary nanocomposites exhibited improved conversion efficiency for NO because gaseous NH_3 and NO are favorable to be absorbed on the surface of the $\text{VO}_x\text{-MnO}_x/\text{CeO}_2$ catalyst. The results of the NH_3 -SCR performance indicated that the NO conversion reached 95% in a wide temperature range of 220–330 °C. Figure 9 shows the possible mechanisms of the $\text{VO}_x\text{-MnO}_x/\text{CeO}_2$ catalyst.

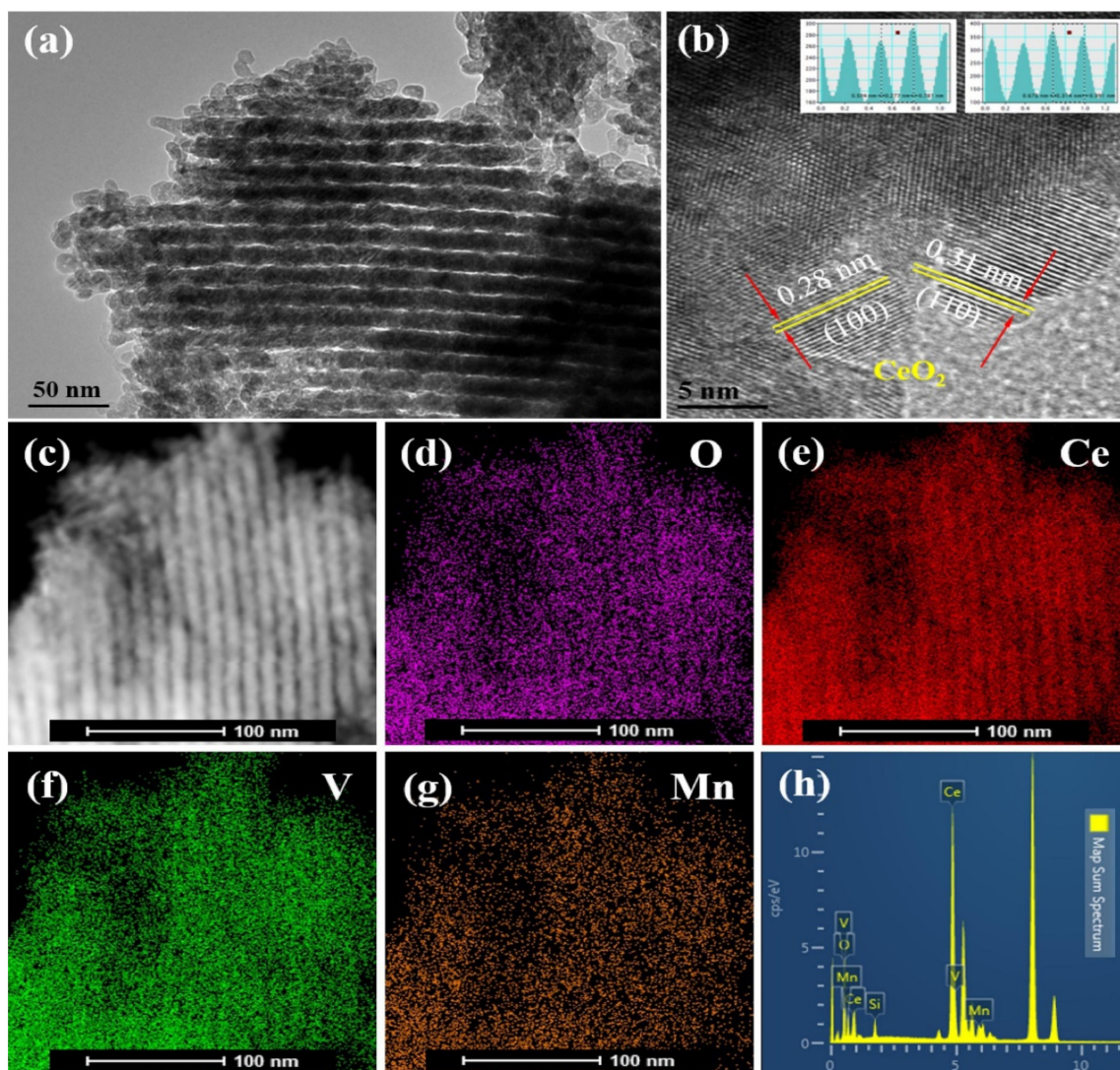


Figure 8. (a) TEM images, (b) HRTEM images, (c–h) energy spectrum analysis (EDS) images and corresponding element mapping of $\text{VO}_x\text{-MnO}_x/\text{CeO}_2$. Reproduced with permission from Reference [30]; copyright (2020), Elsevier.

Wang et al. [60]. evaluated a novel $\text{MnO}_x/\text{CeO}_2/\text{Al}_2\text{O}_3$ ternary catalysts with varying Mn contents through a self-propagating high-temperature synthesis. The characterization results showed that the increasing of the surface atomic concentration improved the activity in the SCR reaction. Moreover, $\text{MnO}_x/\text{CeO}_2/\text{Al}_2\text{O}_3$ possess an extensive pore structure and a large BET surface area to further promote the catalytic performances.

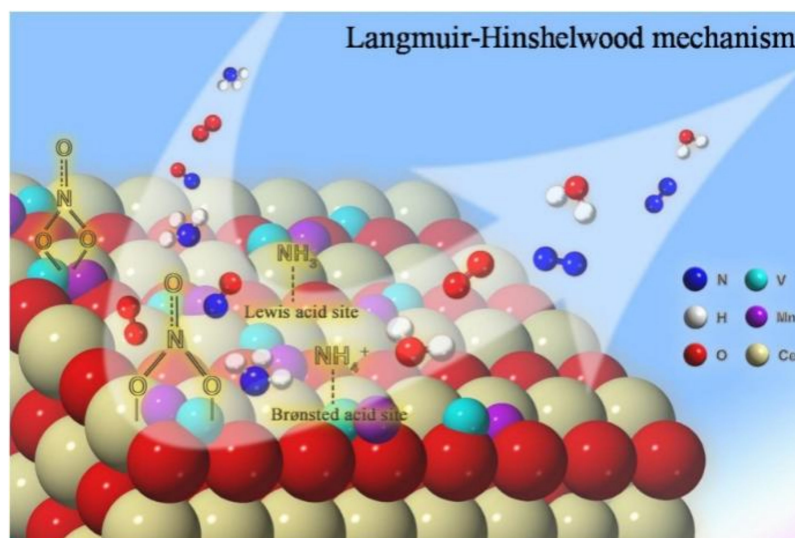


Figure 9. The possible mechanism of the $\text{VO}_x\text{-MnO}_x/\text{CeO}_2$ catalyst. Reproduced with permission from Reference [30]; copyright (2020), Elsevier.

Lee et al. [84] successfully developed $\text{MnO}_x/\text{CeO}_2/\text{TiO}_2$ composites for low-temperature SCR of NO with NH_3 . The Mn/Ce/ TiO_2 (20 wt.% Mn/4 wt.% Ce) catalyst exhibited the highest catalytic activity in the low-temperature range of 120–160 °C, which was mainly attributed to widespread Mn^{4+} dispersion on the surface.

These illustrations of $\text{MnO}_x/\text{CeO}_2$ -based ternary catalysts for SCR of NO_x provided basic perspectives and instructions for their application to air purification and environmental conservation.

6. Conclusions and Perspectives

In summary, the current developments in the preparation and application of $\text{MnO}_x/\text{CeO}_2$ -based ternary catalysts for selective catalytic reduction of NO_x by NH_3 are summarized. Various synthetic routes, such as hydrothermal, precipitation, sol-gel, and impregnation methods for fabricating $\text{MnO}_x/\text{CeO}_2$ -based ternary catalysts have been explored. Their large specific surface areas, abundant active sites, and excellent catalytic performances make them very effective materials for SCR of NO_x with NH_3 . Nevertheless, despite significant improvements in $\text{MnO}_x/\text{CeO}_2$ -based ternary catalysts, there are many challenges to overcome to further enhance their material properties and catalytic reaction mechanisms. Therefore, we offer some insights to consider for future research:

Further analyses are required to determine with the catalytic activity with various morphologies (nanofibers, nanotubes, nanorods) of $\text{MnO}_x/\text{CeO}_2$.

The reaction mechanisms of $\text{MnO}_x/\text{CeO}_2$ catalysts. The effects of catalyst properties (e.g., pore size, porosity, and surface structure) on catalytic activity should be further explored.

Application research should be expanded. Current applications of $\text{MnO}_x/\text{CeO}_2$ -based hybrids are mainly targeted at nitrogen fixation and degradation of formaldehyde. $\text{MnO}_x/\text{CeO}_2$ catalysts can be explored for applications in the degradation of more pollutants, such as in Cr(VI) reduction and CO_2 reduction.

Current research has mainly been done under laboratory conditions. For practical engineering applications, the design of applicable reaction systems for $\text{MnO}_x/\text{CeO}_2$ catalysts is required.

The transfer mechanism of charge carriers needs to be better understood as understanding of the mechanism is helpful to seek more efficient materials that can combine with $\text{MnO}_x/\text{CeO}_2$ to achieve better catalytic activity.

Author Contributions: H.S.: Designing experiment, investigation, optimizing methodology, experimental and data analysis, writing-original draft, review & editing. S.-J.P.: conceptualization, supervision, finalizing, writing-review and editing. All authors have read and agreed to the published version of the manuscript.

Funding: This research was supported by Korea Electric Power Corporation (Grant number: R21XO01-5). This work also supported by the Korea Industrial Complex Corporation through the Project to Program of Industrial Complex Clusters (IRIC2101, Industry-University-Research joint R&D support) funded by the Ministry of Trade, Industry & Energy (MOTIE, Korea).

Conflicts of Interest: The authors declare no conflict of interest.

References

1. Kumar, B.R.; Saravanan, S.; Rana, D.; Anish, V.; Nagendran, A. Effect of a sustainable biofuel-n-octanol-on the combustion, performance and emissions of a DI diesel engine under naturally aspirated and exhaust gas recirculation (EGR) modes. *Energy Convers. Manag.* **2016**, *118*, 275–286. [[CrossRef](#)]
2. Richter, A.; Burrows, J.P.; Nüß, H.; Granier, C.; Niemeier, U. Increase in tropospheric nitrogen dioxide over China observed from space. *Nature* **2005**, *437*, 129–132. [[CrossRef](#)] [[PubMed](#)]
3. Reşitoğlu, İ.A.; Altinişik, K.; Keskin, A. The pollutant emissions from diesel-engine vehicles and exhaust aftertreatment systems. *Clean Technol. Environ. Policy* **2015**, *17*, 15–27. [[CrossRef](#)]
4. Song, W.; Liu, X.Y.; Hu, C.C.; Chen, G.Y.; Liu, X.J. Very low mutation burden is a feature of inflamed recurrent glioblastomas responsive to cancer immunotherapy. *Nat. Commun.* **2021**, *12*, 1–7.
5. Liu, M.; Huang, X.; Song, Y.; Tang, J.; Cao, J.; Zhang, X.; Zhang, Q.; Wang, S.; Xu, T.; Kang, L.; et al. Ammonia emission control in China would mitigate haze pollution and nitrogen deposition, but worsen acid rain. *Proc. Natl. Acad. Sci. USA* **2019**, *116*, 7760–7765. [[CrossRef](#)] [[PubMed](#)]
6. Sun, Y.; Zwolińska, E.; Chmielewski, A.G. Abatement technologies for high concentrations of NO_x and SO₂ removal from exhaust gases: A review. *Crit. Rev. Environ. Sci. Technol.* **2016**, *46*, 119–142. [[CrossRef](#)]
7. Derwent, R.G.; Collins, W.J.; Johnson, C.E.; Stevenson, D.S. Transient behaviour of tropospheric ozone precursors in a global 3-D CTM and their indirect greenhouse effects. *Clim. Change* **2001**, *49*, 463–487. [[CrossRef](#)]
8. Xu, S.C.; Miao, Y.M.; Gao, C.; Long, R.Y.; Chen, H.; Zhao, B.; Wang, S.X. Regional differences in impacts of economic growth and urbanization on air pollutants in China based on provincial panel estimation. *J. Clean. Prod.* **2019**, *208*, 340–352. [[CrossRef](#)]
9. Liu, C.; Yang, M. An empirical analysis of dynamic changes in ecological sustainability and its relationship with urbanization in a coastal city: The case of Xiamen in China. *J. Clean. Prod.* **2020**, *256*, 120482. [[CrossRef](#)]
10. Carslaw, D.C. Evidence of an increasing NO₂/NO_x emissions ratio from road traffic emissions. *Atmospheric Environ.* **2005**, *39*, 4793–4802. [[CrossRef](#)]
11. Seddiek, I.S.; Elgohary, M.M. Eco-friendly selection of ship emissions reduction strategies with emphasis on SO_x and NO_x emissions. *Int. J. Nav. Arch. Ocean* **2014**, *6*, 737–748. [[CrossRef](#)]
12. Chung, S.J.; Pillai, K.C.; Moon, I.S. A sustainable environmentally friendly NO_x removal process using Ag (II)/Ag (I)-mediated electrochemical oxidation. *Sep. Purif. Technol.* **2009**, *65*, 156–163. [[CrossRef](#)]
13. Yao, X.; Zhao, R.; Chen, L.; Du, J.; Tao, C.; Yang, F.; Dong, L. Selective catalytic reduction of NO_x by NH₃ over CeO₂ supported on TiO₂: Comparison of anatase, brookite, and rutile. *Appl. Catal. B* **2017**, *208*, 82–93. [[CrossRef](#)]
14. Xie, L.; Liu, F.; Shi, X.; Xiao, F.S.; He, H. Effects of post-treatment method and Na co-cation on the hydrothermal stability of Cu-SSZ-13 catalyst for the selective catalytic reduction of NO_x with NH₃. *Appl. Catal. B* **2015**, *179*, 206–212. [[CrossRef](#)]
15. Li, X.; Li, K.; Peng, Y.; Li, X.; Zhang, Y.; Wang, D.; Chen, J.; Li, J. Interaction of phosphorus with a FeTiOx catalyst for selective catalytic reduction of NO_x with NH₃: Influence on surface acidity and SCR mechanism. *Chem. Eng. J.* **2018**, *347*, 173–183. [[CrossRef](#)]
16. Zong, L.; Zhang, G.; Zhao, J.; Dong, F.; Zhang, J.; Tang, Z. Morphology-controlled synthesis of 3D flower-like TiO₂ and the superior performance for selective catalytic reduction of NO_x with NH₃. *Chem. Eng. J.* **2018**, *343*, 500–511. [[CrossRef](#)]
17. Wang, Q.; Xu, H.; Huang, W.; Pan, Z.; Zhou, H. Metal organic frameworks-assisted fabrication of CuO/Cu₂O for enhanced selective catalytic reduction of NO_x by NH₃ at low temperatures. *J. Hazard. Mater.* **2019**, *364*, 499–508. [[CrossRef](#)]
18. Gómez-García, M.A.; Pitchon, V.; Kiennemann, A. Pollution by nitrogen oxides: An approach to NO_x abatement by using sorbing catalytic materials. *Environ. Int.* **2005**, *31*, 445–467. [[CrossRef](#)]
19. Han, K.; Luo, J.; Feng, Y.; Lai, Q.; Bai, Y.; Tang, W.; Wang, Z.L. Wind-driven radial-engine-shaped triboelectric nanogenerators for self-powered absorption and degradation of NO_x. *ACS Nano* **2020**, *14*, 2751–2759. [[CrossRef](#)] [[PubMed](#)]
20. Yan, R.; Lin, S.; Li, Y.; Liu, W.; Mi, Y.; Tang, C.; Wang, L.; Wu, P.; Peng, H. Novel shielding and synergy effects of Mn-Ce oxides confined in mesoporous zeolite for low temperature selective catalytic reduction of NO_x with enhanced SO₂/H₂O tolerance. *J. Hazard. Mater.* **2020**, *396*, 122592. [[CrossRef](#)]
21. Wang, J.; Zhao, H.; Haller, G.; Li, Y. Recent advances in the selective catalytic reduction of NO_x with NH₃ on Cu-Chabazite catalysts. *Appl. Catal. B* **2017**, *202*, 346–354. [[CrossRef](#)]

22. Bai, Y.; Dong, J.; Hou, Y.; Guo, Y.; Liu, Y.; Li, Y.; Han, X.; Huang, Z. Co₃O₄@PC derived from ZIF-67 as an efficient catalyst for the selective catalytic reduction of NO_x with NH₃ at low temperature. *Chem. Eng. J.* **2019**, *361*, 703–712. [[CrossRef](#)]
23. Kwon, D.W.; Park, K.H.; Ha, H.P.; Hong, S.C. The role of molybdenum on the enhanced performance and SO₂ resistance of V/Mo-Ti catalysts for NH₃-SCR. *Appl. Surf. Sci.* **2019**, *481*, 1167–1177. [[CrossRef](#)]
24. Saramok, M.; Szymaszek, A.; Inger, M.; Jurak, K.A.; Samojeden, B.; Motak, M. Modified Zeolite Catalyst for a NO_x Selective Catalytic Reduction Process in Nitric Acid Plants. *Catalysts* **2021**, *11*, 450. [[CrossRef](#)]
25. You, X.; Sheng, Z.; Yu, D.; Yang, L.; Xiao, X.; Wang, S. Influence of Mn/Ce ratio on the physicochemical properties and catalytic performance of graphene supported MnO_x-CeO₂ oxides for NH₃-SCR at low temperature. *Appl. Surf. Sci.* **2017**, *423*, 845–854. [[CrossRef](#)]
26. Liu, C.; Gao, G.; Shi, J.W.; He, C.; Li, G.; Bai, N.; Niu, C. MnO_x-CeO₂ shell-in-shell microspheres for NH₃-SCR de-NO_x at low temperature. *Catal. Commun.* **2016**, *86*, 36–40. [[CrossRef](#)]
27. Qi, G.; Yang, R.T.; Chang, R. MnO_x-CeO₂ mixed oxides prepared by co-precipitation for selective catalytic reduction of NO with NH₃ at low temperatures. *Appl. Catal. B* **2004**, *51*, 93–106. [[CrossRef](#)]
28. Qi, G.; Yang, R.T. Performance and kinetics study for low-temperature SCR of NO with NH₃ over MnO_x-CeO₂ catalyst. *J. Catal.* **2003**, *217*, 434–441. [[CrossRef](#)]
29. Ye, L.; Lu, P.; Peng, Y.; Li, J.; Huang, H. Impact of NO_x and NH₃ addition on toluene oxidation over MnO_x-CeO₂ catalyst. *J. Hazard. Mater.* **2021**, *416*, 125939. [[CrossRef](#)]
30. Wu, X.; Chen, Z.; Yu, X.; Huang, Z.; Shen, H.; Jing, G. Mechanism by which three-dimensional ordered mesoporous CeO₂ promotes the activity of VO_x-MnO_x/CeO₂ catalysts for NO_x abatement: Atomic-scale insight into the catalytic cycle. *Chem. Eng. J.* **2020**, *399*, 125629. [[CrossRef](#)]
31. Andreoli, S.; Deorsola, F.A.; Pirone, R. MnO_x-CeO₂ catalysts synthesized by solution combustion synthesis for the low-temperature NH₃-SCR. *Catal. Today* **2015**, *253*, 199–206. [[CrossRef](#)]
32. Zhang, H.; Yuan, S.; Wang, J.L.; Gong, M.; Chen, Y. Effects of contact model and NO_x on soot oxidation activity over Pt/MnO_x-CeO₂ and the reaction mechanisms. *Chem. Eng. J.* **2017**, *327*, 1066–1076. [[CrossRef](#)]
33. Delimaris, D.; Ioannides, T. VOC oxidation over MnO_x-CeO₂ catalysts prepared by a combustion method. *Appl. Catal. B* **2008**, *84*, 303–312. [[CrossRef](#)]
34. Sun, H.; Yu, X.; Ma, X.; Yang, X.; Lin, M.; Ge, M. MnO_x-CeO₂ catalyst derived from metal-organic frameworks for toluene oxidation. *Catal. Today* **2019**, *35*, 580–586. [[CrossRef](#)]
35. Li, C.; Tang, X.; Yi, H.; Wang, L.; Cui, X.; Chu, C.; Li, J.; Zhang, R.; Yu, Q. Rational design of template-free MnO_x-CeO₂ hollow nanotube as de-NO_x catalyst at low temperature. *Appl. Surf. Sci.* **2018**, *428*, 924–932. [[CrossRef](#)]
36. Shen, B.; Wang, F.; Liu, T. Homogeneous MnO_x-CeO₂ pellets prepared by a one-step hydrolysis process for low-temperature NH₃-SCR. *Powder Technol.* **2014**, *253*, 152–157. [[CrossRef](#)]
37. Tikhomirov, K.; Kröcher, O.; Elsener, M.; Wokaun, A. MnO_x-CeO₂ mixed oxides for the low-temperature oxidation of diesel soot. *Appl. Catal. B* **2006**, *64*, 72–78. [[CrossRef](#)]
38. Cui, M.; Li, Y.; Wang, X.; Wang, J.; Shen, M. Effect of preparation method on MnO_x-CeO₂ catalysts for NO oxidation. *J. Rare Earths.* **2013**, *31*, 572–576. [[CrossRef](#)]
39. Li, H.; Wu, C.Y.; Li, Y.; Li, L.; Zhao, Y.; Zhang, J. Role of flue gas components in mercury oxidation over TiO₂ supported MnO_x-CeO₂ mixed-oxide at low temperature. *J. Hazard. Mater.* **2012**, *243*, 117–123. [[CrossRef](#)]
40. Wang, X.; Kang, Q.; Li, D. Catalytic combustion of chlorobenzene over MnO_x-CeO₂ mixed oxide catalysts. *Appl. Catal. B* **2009**, *86*, 166–175.
41. Kong, Z.; Li, Y.; Wang, Y.; Zhang, Y.; Shen, K.; Chu, X.; Wang, H.; Wang, J.; Zhan, L. Monodispersed MnO_x-CeO₂ solid solution as superior electrocatalyst for Li₂S precipitation and conversion. *Chem. Eng. J.* **2020**, *392*, 123697. [[CrossRef](#)]
42. Tang, X.; Chen, J.; Huang, X.; Xu, Y.; Shen, W. Pt/MnO_x-CeO₂ catalysts for the complete oxidation of formaldehyde at ambient temperature. *Appl. Catal. B* **2008**, *81*, 115–121. [[CrossRef](#)]
43. Xie, Y.; Li, C.; Zhao, L.; Zhang, J.; Zeng, G.; Zhang, X.; Zhang, W.; Tao, S. Experimental study on Hg⁰ removal from flue gas over columnar MnO_x-CeO₂/activated coke. *Appl. Surf. Sci.* **2015**, *333*, 59–67. [[CrossRef](#)]
44. Meng, Q.; Cui, J.; Wang, K.; Tang, Y.; Zhao, K.; Huang, L. Facile preparation of hollow MnO_x-CeO₂ composites with low Ce content and their catalytic performance in NO oxidation. *Mol. Catal.* **2020**, *493*, 111107. [[CrossRef](#)]
45. Yao, X.; Ma, K.; Zou, W.; He, S.; An, J.; Yang, F.; Dong, L. Influence of preparation methods on the physicochemical properties and catalytic performance of MnO_x-CeO₂ catalysts for NH₃-SCR at low temperature. *Chinese J. Catal.* **2017**, *38*, 146–159. [[CrossRef](#)]
46. Xu, H.; Zhang, Q.; Qiu, C.; Lin, T.; Gong, M.; Chen, Y. Tungsten modified MnO_x-CeO₂/ZrO₂ monolith catalysts for selective catalytic reduction of NO_x with ammonia. *Chem. Eng. Sci.* **2012**, *76*, 120–128. [[CrossRef](#)]
47. Sun, H.; Park, S.J. Phosphorus-doped g-C₃N₄/SnS nanocomposite for efficient photocatalytic reduction of aqueous Cr (VI) under visible light. *Appl. Surf. Sci.* **2020**, *531*, 147325. [[CrossRef](#)]
48. Zhang, P.; Lou, X.W. Design of Heterostructured Hollow Photocatalysts for Solar-to-Chemical Energy Conversion. *Adv. Mater.* **2019**, *31*, 1900281. [[CrossRef](#)] [[PubMed](#)]
49. Wang, Z.; Lv, J.; Zhang, J.; Dai, K.; Liang, C. Facile synthesis of Z-scheme BiVO₄/porous graphite carbon nitride heterojunction for enhanced visible-light-driven photocatalyst. *Appl. Surf. Sci.* **2018**, *430*, 595–602. [[CrossRef](#)]

50. Yang, X.; Tian, L.; Zhao, X.; Tang, H.; Liu, Q.; Li, G.X. Interfacial optimization of g-C₃N₄-based Z-scheme heterojunction toward synergistic enhancement of solar-driven photocatalytic oxygen evolution. *Appl. Catal. B* **2019**, *244*, 240–249. [[CrossRef](#)]
51. Marschall, R. Semiconductor composites: Strategies for enhancing charge carrier separation to improve photocatalytic activity. *Adv. Funct. Mater.* **2014**, *24*, 2421–2440. [[CrossRef](#)]
52. Liang, Y.; Guo, N.; Li, L.; Li, R.; Ji, G.; Gan, S. Fabrication of porous 3D flower-like Ag/ZnO heterostructure composites with enhanced photocatalytic performance. *Appl. Surf. Sci.* **2015**, *332*, 32–39. [[CrossRef](#)]
53. Di, L.; Yang, H.; Xian, T.; Liu, X.; Chen, X. Photocatalytic and photo-Fenton catalytic degradation activities of Z-scheme Ag₂S/BiFeO₃ heterojunction composites under visible-light irradiation. *Nanomaterials* **2019**, *9*, 399. [[CrossRef](#)] [[PubMed](#)]
54. El-Bery, H.M.; Matsushita, Y.; Abdel-moneim, A. Fabrication of efficient TiO₂-RGO heterojunction composites for hydrogen generation via water-splitting: Comparison between RGO, Au and Pt reduction sites. *Appl. Surf. Sci.* **2017**, *423*, 185–196. [[CrossRef](#)]
55. Song, H.; Wu, R.; Yang, J.; Dong, J.; Ji, G. Fabrication of CeO₂ nanoparticles decorated three-dimensional flower-like BiOI composites to build pn heterojunction with highly enhanced visible-light photocatalytic performance. *J. Colloid Interface Sci.* **2018**, *512*, 325–334. [[CrossRef](#)] [[PubMed](#)]
56. Wang, Q.; Wang, W.; Zhong, L.; Liu, D.; Cao, X.; Cui, F. Oxygen vacancy-rich 2D/2D BiOCl-g-C₃N₄ ultrathin heterostructure nanosheets for enhanced visible-light-driven photocatalytic activity in environmental remediation. *Appl. Catal. B* **2018**, *220*, 290–302. [[CrossRef](#)]
57. Li, L.; Yu, X.; Xu, L.; Zhao, Y. Fabrication of a novel type visible-light-driven heterojunction photocatalyst: Metal-porphyrinic metal organic framework coupled with PW12/TiO₂. *Chem. Eng. J.* **2020**, *386*, 123955. [[CrossRef](#)]
58. Dutta, V.; Sharma, S.; Raizada, P.; Thakur, V.K.; Khan, A.A.P.; Saini, V.; Asiri, A.M.; Singh, P.V. An Overview on WO₃ based photocatalyst for environmental remediation, *J. Environ. Chem. Eng.* **2021**, *9*, 105018.
59. Li, H.; Wu, C.Y.; Li, Y.; Zhang, J. Superior activity of MnO_x-CeO₂/TiO₂ catalyst for catalytic oxidation of elemental mercury at low flue gas temperatures. *Appl. Catal. B* **2012**, *111*, 381–388. [[CrossRef](#)]
60. Wang, C.; Yu, F.; Zhu, M.; Tang, C.; Zhang, K.; Zhao, D.; Dong, L.; Dai, B. Bin. Dai, Highly selective catalytic reduction of NO_x by MnO_x-CeO₂-Al₂O₃ catalysts prepared by self-propagating high-temperature synthesis. *J. Environ. Sci.* **2019**, *75*, 124–135. [[CrossRef](#)] [[PubMed](#)]
61. Ye, L.; Lu, P.; Chen, X.; Fang, P.; Peng, Y.; Li, J.; Huang, H. The deactivation mechanism of toluene on MnO_x-CeO₂ SCR catalyst. *Appl. Catal. B* **2020**, *277*, 119257. [[CrossRef](#)]
62. Li, W.; Liu, H.; Chen, Y. Mesoporous MnO_x-CeO₂ composites for NH₃-SCR: The effect of preparation methods and a third dopant. *RSC Adv.* **2019**, *9*, 11912–11921.
63. Li, L.; Sun, B.; Sun, J.; Yu, S.; Ge, C.; Tang, C.; Dong, L. Novel MnO_x-CeO₂ nanosphere catalyst for low-temperature NH₃-SCR. *Catal Commun.* **2017**, *100*, 98–102. [[CrossRef](#)]
64. Li, S.; Huang, B.; Yu, C. A CeO₂-MnO_x core-shell catalyst for low-temperature NH₃-SCR of NO. *Catal. Commun.* **2017**, *98*, 47–51. [[CrossRef](#)]
65. Yao, X.; Chen, L.; Cao, J.; Chen, Y.; Tian, M.; Yang, F.; Sun, J.; Tang, C.; Dong, L. Enhancing the deNO_x performance of MnO_x/CeO₂-ZrO₂ nanorod catalyst for low-temperature NH₃-SCR by TiO₂ modification. *Chem. Eng. J.* **2019**, *369*, 46–56. [[CrossRef](#)]
66. Anthonysamy, S.B.I.; Afandi, S.B.; Khavarian, M.; Mohamed, A.R.B. A review of carbon-based and non-carbon-based catalyst supports for the selective catalytic reduction of nitric oxide. *Beilstein J. Nanotechnol.* **2018**, *9*, 740–761. [[CrossRef](#)]
67. Ma, L.; Seo, C.Y.; Nahata, M.; Chen, X.; Li, J.; Schwank, J.W. Shape dependence and sulfate promotion of CeO₂ for selective catalytic reduction of NO_x with NH₃. *Appl. Catal. B* **2018**, *232*, 246–259. [[CrossRef](#)]
68. Liu, C.; Shi, J.W.; Gao, C.; Niu, C. Manganese oxide-based catalysts for low-temperature selective catalytic reduction of NO_x with NH₃: A review. *Appl. Catal. A Gen.* **2016**, *522*, 54–69. [[CrossRef](#)]
69. Ma, Z.; Weng, D.; Wu, X.; Si, Z. Effects of WO_x modification on the activity, adsorption and redox properties of CeO₂ catalyst for NO_x reduction with ammonia. *J. Environ. Sci.* **2012**, *24*, 1305–1316. [[CrossRef](#)]
70. Chatterjee, D.; Burkhardt, T.; Weibel, M.; Tronconi, E.; Nova, I.; Ciardelli, C. *Numerical Simulation of NO/NO₂/NH₃ Reactions on SCR-Catalytic Converters: Model Development and Applications*; SAE Technical Paper No. 2006-01-0468; SAE International: Warrendale, PA, USA, 2006.
71. Xu, Y.; Wu, X.; Lin, Q.; Hu, J.; Ran, R.; Weng, D. SO₂ promoted V₂O₅-MoO₃/TiO₂ catalyst for NH₃-SCR of NO_x at low temperatures. *Appl. Catal. A Gen.* **2019**, *570*, 42–50. [[CrossRef](#)]
72. Jiang, Y.; Gao, J.; Zhang, Q.; Liu, Z.; Fu, M.; Wu, J.; Hu, Y.; Ye, D. Enhanced oxygen vacancies to improve ethyl acetate oxidation over MnO_x-CeO₂ catalyst derived from MOF template. *Chem. Eng. J.* **2019**, *371*, 78–87. [[CrossRef](#)]
73. Sudarsanam, P.; Hillary, B.; Amin, M.H.; Abd Hamid, S.B.; Bhargava, S.K. Structure-activity relationships of nanoscale MnO_x/CeO₂ heterostructured catalysts for selective oxidation of amines under eco-friendly conditions. *Appl. Catal. B* **2016**, *185*, 213–224. [[CrossRef](#)]
74. Zhou, C.; Zhang, H.; Zhang, Z.; Li, L. Improved reactivity for toluene oxidation on MnO_x/CeO₂-ZrO₂ catalyst by the synthesis of cubic-tetragonal interfaces. *Appl. Surf. Sci.* **2021**, *539*, 148188. [[CrossRef](#)]
75. Zhu, K.; Yan, W.; Liu, S.; Wu, X.; Cui, S.; Shen, X. One-step hydrothermal synthesis of MnO_x-CeO₂/reduced graphene oxide composite aerogels for low temperature selective catalytic reduction of NO_x. *Appl. Surf. Sci.* **2020**, *508*, 145024. [[CrossRef](#)]

76. Chang, H.; Li, J.; Chen, X.; Ma, L.; Yang, S.; Schwank, J.W.; Hao, J. Effect of Sn on MnO_x-CeO₂ catalyst for SCR of NO_x by ammonia: Enhancement of activity and remarkable resistance to SO₂. *Catal. Commun.* **2012**, *27*, 54–57. [[CrossRef](#)]
77. Lin, F.; Wu, X.; Liu, S.; Weng, D.; Huang, Y. Preparation of MnO_x-CeO₂-Al₂O₃ mixed oxides for NO_x-assisted soot oxidation: Activity, structure and thermal stability. *Chem. Eng. J.* **2013**, *226*, 105–112. [[CrossRef](#)]
78. Zhang, H.; Gu, F.; Liu, Q.; Gao, J.; Jia, L.; Zhu, T.; Chen, Y.; Zhong, Z.; Su, F. MnO_x-CeO₂ supported on a three-dimensional and networked SBA-15 monolith for NO_x-assisted soot combustion. *RSC Adv.* **2014**, *4*, 14879–14889. [[CrossRef](#)]
79. Guo, L.; Meng, F.; Zeng, Y.; Jia, Y.; Qian, F.; Zhang, S.; Zhong, Q. Catalytic ozonation of NO_x into HNO₃ with low concentration ozone over MnO_x-CeO₂/TiO₂: Two-phase synergistic effect of TiO₂. *Mol. Catal.* **2020**, *493*, 111095. [[CrossRef](#)]
80. Liu, Q.; Fu, Z.; Ma, L.; Niu, H.; Liu, C.; Li, J.; Zhang, Z. MnO_x-CeO₂ supported on Cu-SSZ-13: A novel SCR catalyst in a wide temperature range. *Appl. Catal. A Gen.* **2017**, *547*, 146–154. [[CrossRef](#)]
81. Ma, D.; Yang, L.; Huang, B.; Wang, L.; Wang, X.; Sheng, Z.; Dong, F. MnO_x-CeO₂@TiO₂ core-shell composites for low temperature SCR of NO_x. *N. J. Chem.* **2019**, *43*, 15161–15168. [[CrossRef](#)]
82. Zhang, L.; Cui, S.; Guo, H.; Ma, X.; Luo, X. The influence of K⁺ cation on the MnO_x-CeO₂/TiO₂ catalysts for selective catalytic reduction of NO_x with NH₃ at low temperature. *J. Mol. Catal. A-Chem.* **2014**, *390*, 14–21. [[CrossRef](#)]
83. Wu, X.; Yu, X.; Huang, Z.; Shen, H.; Jing, G. MnO_x-decorated VO_x/CeO₂ catalysts with preferentially exposed {110} facets for selective catalytic reduction of NO_x by NH₃. *Appl. Catal. B* **2020**, *268*, 118419. [[CrossRef](#)]
84. Lee, S.M.; Park, K.H.; Hong, S.C. MnO_x/CeO₂-TiO₂ mixed oxide catalysts for the selective catalytic reduction of NO with NH₃ at low temperature. *Chem. Eng. J.* **2012**, *195*, 323–331. [[CrossRef](#)]
85. Sun, L.; Shao, R.; Chen, Z.; Tang, L.; Dai, Y.; Ding, J. Alkali-dependent synthesis of flower-like ZnO structures with enhanced photocatalytic activity via a facile hydrothermal method. *Appl. Surf. Sci.* **2012**, *258*, 5455–5461. [[CrossRef](#)]
86. Dong, W.; Wang, X.; Li, B.; Wang, L.; Chen, B.; Li, C.; Li, X.; Zhang, T.; Shi, Z. Hydrothermal synthesis and structure evolution of hierarchical cobalt sulfide nanostructures. *Dalton Trans.* **2011**, *40*, 243–248. [[CrossRef](#)]
87. Zhang, P.; Yin, S.; Sato, T. Synthesis of high-activity TiO₂ photocatalyst via environmentally friendly and novel microwave assisted hydrothermal process. *Appl. Catal. B* **2009**, *89*, 118–122. [[CrossRef](#)]
88. Wang, X.; Xu, H.; Wang, H.; Yan, H. Morphology-controlled BaWO₄ powders via a template-free precipitation technique. *J. Cryst. Growth* **2005**, *284*, 254–261. [[CrossRef](#)]
89. Yuan, Z.; Li, R.; Meng, F.; Zhang, J.; Zuo, K.; Han, E. Approaches to enhancing gas sensing properties: A review. *Sensors* **2019**, *19*, 1495. [[CrossRef](#)] [[PubMed](#)]
90. Bhargava, R.; Khan, S. Effect of reduced graphene oxide (rGO) on structural, optical, and dielectric properties of Mg(OH)₂/rGO nanocomposites. *Adv. Powder Technol.* **2017**, *28*, 2812–2819. [[CrossRef](#)]
91. Zhang, Y.; Huo, Q.Y.; Du, P.P.; Wang, L.Z.; Zhang, A.Q.; Song, Y.H.; Lv, Y.; Li, G.Y. Advances in new cathode material LiFePO₄ for lithium-ion batteries. *Synth. Met.* **2012**, *162*, 1315–1326. [[CrossRef](#)]
92. Amri, A.; Jiang, Z.T.; Pryor, T.; Yin, C.Y.; Djordjevic, S. Developments in the synthesis of flat plate solar selective absorber materials via sol-gel methods: A review. *Renew. Sust. Energ. Rev.* **2014**, *36*, 316–328. [[CrossRef](#)]
93. He, F.; Wang, X.; Wu, D. New approach for sol-gel synthesis of microencapsulated n-octadecane phase change material with silica wall using sodium silicate precursor. *Energy* **2014**, *67*, 223–233. [[CrossRef](#)]
94. Zegeye, T.A.; Tsai, M.C.; Cheng, J.H.; Lin, M.H.; Chen, H.M.; Rick, J.; Su, W.N.; Jeffrey Kuo, C.F.; Hwang, B.J. Controllable embedding of sulfur in high surface area nitrogen doped three dimensional reduced graphene oxide by solution drop impregnation method for high performance lithium-sulfur batteries. *J. Power Sources* **2017**, *353*, 298–311. [[CrossRef](#)]
95. Chen, X.; Gao, H.; Yang, M.; Dong, W.; Huang, X.; Li, A.; Dong, C.; Wang, G. Highly graphitized 3D network carbon for shape-stabilized composite PCMs with superior thermal energy harvesting. *Nano Energy* **2018**, *49*, 86–94. [[CrossRef](#)]
96. Huang, X.; Shen, T.; Zhang, T.; Qiu, H.; Gu, X.; Ali, Z.; Hou, Y. Efficient oxygen reduction catalysts of porous carbon nanostructures decorated with transition metal species. *Adv. Energy Mater.* **2020**, *10*, 1900375. [[CrossRef](#)]
97. Wu, X.; Liu, S.; Lin, F.; Weng, D. Nitrate storage behavior of Ba/MnO_x-CeO₂ catalyst and its activity for soot oxidation with heat transfer limitations. *J. Hazard. Mater.* **2010**, *181*, 722–728. [[CrossRef](#)] [[PubMed](#)]
98. Ding, L.; Liu, C.; Chen, K.; Huang, Y.; Diao, B. Atmospheric pollution reduction effect and regional predicament: An empirical analysis based on the Chinese provincial NO_x emissions. *J. Environ. Manag.* **2017**, *196*, 178–187. [[CrossRef](#)]
99. Obradović, B.M.; Sretenović, G.B.; Kuraica, M.M. A dual-use of DBD plasma for simultaneous NO_x and SO₂ removal from coal-combustion flue gas. *J. Hazard. Mater.* **2011**, *185*, 1280–1286. [[CrossRef](#)]
100. Song, C.L.; Bin, F.; Tao, Z.M.; Li, F.C.; Huang, Q.F. Simultaneous removals of NO_x, HC and PM from diesel exhaust emissions by dielectric barrier discharges. *J. Hazard. Mater.* **2009**, *166*, 523–530. [[CrossRef](#)]
101. Park, S.J.; Kim, B.J. A study on NO removal of activated carbon fibers with deposited silver nanoparticles. *J. Colloid Interface Sci.* **2005**, *282*, 124–127. [[CrossRef](#)] [[PubMed](#)]
102. Park, S.J.; Kim, J.J.; Kim, M.J.; Park, R.J.; Cheong, H.B. Characteristics of flow and reactive pollutant dispersion in urban street canyons Cheong. *Atmospheric Environ.* **2015**, *108*, 20–31. [[CrossRef](#)]
103. Park, B.J.; Park, S.J.; Ryu, S.K.J. Removal of NO over copper supported on activated carbon prepared by electroless plating. *J. Colloid Interface Sci.* **1999**, *217*, 142–145. [[CrossRef](#)] [[PubMed](#)]

-
104. Park, S.J.; Kim, B.J. Oxidation behaviors of metallic copper particles in NO reduction mechanism of copper/activated carbons. *J. Colloid Interface Sci.* **2005**, *292*, 493–497. [[CrossRef](#)] [[PubMed](#)]
 105. Wu, X.; Liu, S.; Weng, D.; Lin, F.; Rin, R. MnO_x-CeO₂-Al₂O₃ mixed oxides for soot oxidation: Activity and thermal stability. *J. Hazard. Mater.* **2011**, *187*, 283–290. [[CrossRef](#)] [[PubMed](#)]